

A Dynamic Inflow-Based Induced Power Model for General and Optimal Rotor Performance

JunSoo Hong
jh25@wustl.edu

Graduate Research Assistant

David A. Peters
dap@wustl.edu

McDonnell Douglas Professor

Washington University
 St. Louis, Missouri

Robert A. Ormiston
robert.a.ormiston2.vol@mail.mil

Emeritus Scientist

US Army Aviation Development
 Directorate Aviation & Missile
 Research, Development &
 Engineering Center Moffett
 Field, California

ABSTRACT

A rigorous analytical model for lifting rotor performance in forward flight is developed that combines finite state Dynamic Inflow theory with conventional blade element theory. Dynamic Inflow is based on first-principles potential flow theory that relates the rotor induced inflow velocity distribution to the rotor pressure loading. The model is able to capture increased induced power at higher advance ratios not predicted by Glauert's classical momentum theory. The model provides general performance characteristics for specified blade pitch and radial twist control as well as optimum performance subject to specified constraints. The rotor is treated as an infinite-blade actuator disk including the effects of reverse flow and inflow feedback. Results confirm the singularity in rotor power found in earlier investigations and provides new understanding of the important effects of reverse flow, inflow feedback, rotor solidity, and blade root cutout. The model also directly yields power constants for a quadratic power model that may be used to quickly calculate induced power as a function of advance ratio. Results obtained using higher harmonic blade pitch control show that induced power is reduced for all conditions. With a sufficient number of control degrees of freedom, induced power approaches Glauert's minimum ideal power. Higher harmonic control also eliminates the infinite power singularity.

NOTATION

a	slope of lift curve, rad^{-1}	$[\bar{L}^e]$	matrix relating pressure state to inflow state
A	rotor disk area	$[\bar{L}^e]_{sym}$	symmetric part of $[\bar{L}^e]$
$[\bar{A}]$	effect of control input	M	maximum harmonic number of Dynamic Inflow states
$[\bar{B}]$	effect of inflow feedback	N	number of polynomials used in the expansion of radial inflow function
$\{C\}$	rotor loading constraints	ΔP	non-dimensional pressure difference
$\{\bar{C}\}$	normalized loading constraints, $\{C\}/C_T$	$P_n^m(\nu)$	normalized Legendre function
c	blade chord	$[\bar{P}]$	matrix relating pressure states to control variables
C_L	roll moment coefficient	R	blade radius
C_M	pitch moment coefficient	rco	root cutout, fraction of blade radius
C_P	induced power coefficient	\bar{r}	non-dimensional radial position
C_T	thrust coefficient	t	time
D	maximum order of blade radial twist control polynomial	$[U]$	flipping matrix
$[\bar{D}]$	matrix relating pressure states to rotor loads	U_T	blade section tangential velocity component
$F()$	functional	U_P	blade section perpendicular velocity component
H	maximum harmonic of blade pitch control	V	$\sqrt{\mu^2 + \lambda^2}$
$[I]$	identity matrix	V_∞	non-dimensional free-stream velocity
L_q	blade airload, lift per unit length		

$w(\bar{r}, \psi)$	non-dimensional induced flow
α_s	nose up shaft angle
$\{\gamma\}$	inflow state
$\theta(\bar{r}, \psi)$	blade pitch angle
$\{\theta\}$	rotor control
λ	inflow due to shaft tilt = $-\mu\alpha$
$\{\bar{\Lambda}\}$	Lagrange multiplier
μ	advance ratio = $V\sin(\chi)$
ν	ellipsoidal coordinate
ρ	air density
σ	solidity, $bc/\pi R$
$\{\bar{r}\}$	pressure states
$\phi_n^m(\bar{r})$	inflow expansion function
χ	wake skew angle
ψ	azimuth angle
Ω	rotor speed

INTRODUCTION

The induced velocity field of a lifting rotor in forward flight is fundamental problem in rotorcraft aerodynamics, Ref. [1]. The radial and azimuthal non-uniformities of the induced velocity produce significant unsteady blade air loads that influence nearly all important rotorcraft characteristic such as rotor lift, drag, and power, rotor trim and control, blade structural loads, vehicle vibration, and acoustics. Modeling of the induced velocity field is inherently difficult because of its mutual dependence on the non-uniform rotor blade air load distribution. By contrast, modeling of the analogous problem for the fixed wing is relatively easy. Prandtl-Glauert lifting line theory is straight forward to use and it can provide reasonable solutions for the fixed wing problem.

This paper addresses the influence of induced velocity on rotor performance, that is, the lift, drag, and power of a lifting rotor in forward flight. Elementary momentum theory uses uniform inflow. Therefore, it provides an overly simplistic model for lifting rotor induced power. More accurate representations are available but these rely on elaborate discrete vortex filament models or newer computational fluid dynamics (CFD) methods.

References 2 and 3 provide an alternative to the existing overly simplistic or computationally intensive approaches. This method is called Finite-State Rotor Inflow Theory, or Dynamic Inflow and it is developed by Peters and He in Ref. [4]. Dynamic Inflow is based on rigorous potential flow theory specialized to the lifting rotor in axial or edgewise flow.

The present paper is an extension of Refs. [2], [3], therefore, Dynamic Inflow is used throughout this present paper. The result is a compact model that yields rotor induced power for

1) the general performance problem of determining power for specified rotor controls.

2) the inverse problem of determining the optimum controls variables for minimum power.

The analytical nature of the present theory also provides important insights into the nature of the rotor induced power and its behavior as a function of operating conditions and configuration variables.

Interest in rotor induced power derives from the ever-present desire to improve rotorcraft performance and efficiency, particularly at high speed. Harris review paper (Ref. [5]) highlighted the widely underappreciated inaccuracy of Glauert's simplified momentum theory at high advance ratios by showing that induced power increased significantly rather than decreased with advance ratio. Subsequently, Ormiston used Dynamic Inflow and vortex wake models to reinforce these results in Refs. [6], [7]. In these papers, he also showed the existence of a singularity in rotor induced power for advance ratio near 1.0 for a rotor trimmed to zero pitch and roll moments under certain rotor loading conditions.

Ormiston later postulated a linear quadratic induced power model in terms of control variables for rotor angle of attack, collective pitch, and blade twist in Ref. [8]. Power constants were deduced as a function of advance ratio using computed results from Dynamic inflow. The model was used to determine the optimum controls for minimum power. Limited study of applying higher harmonic blade pitch control (HHC) showed additional reduction in induced power.

These results provided the impetus to derive the analytical rotor power model directly from Dynamic Inflow theory. This avoided cumbersome numerical identification of the power constants and greatly increased flexibility, generality and utility of the model, not to mention increased insight, elegance and accuracy. The first step was reported by File et al in Ref. [2]

1) general performance problem.

2) optimization for minimum power.

It may be noted that the work of Garcia-Duffy et al in Ref. [9] was a precursor to Ref. [2].

Preliminary results were presented in Ref. [2] although they did not include the effects of reverse flow, inflow feedback, and a finite number of blades. In the present study, the important effects of reverse flow and inflow feedback are now included although the infinite-blade actuator disk model is retained. The present refinements now enable confirmation of key results identified by Ormiston, specifically the induced power singularity.

Other relevant investigations of rotor induced power were conducted by Hall, et al in Refs. [10], [11]. This work employed a discretized, linear, vortex lattice model to determine the optimum induced power of finite-bladed rotors. No constraints on blade controls or planform geometry (a "rubber blade") were used to determine the optimum induced power. They also studied the effects of specified conventional and higher harmonic blade pitch on induced power. The results generally confirmed the findings of Ormiston and File.

THEORY

Finite-State Induced-Inflow Theory

The following development generally follows Ref. [2]. According to the Peter/He theory, inflow and pressure distribution across the disk can be represented as inflow and pressure states, $\{\gamma\}$ and $\{\bar{\tau}\}$, Ref. [4]

$$(1) \quad w(\bar{r}, \psi) = \sum_{r=-\infty}^{+\infty} \sum_{j=|r|+1, |r|+3, \dots}^{+\infty} \phi_j^r(\bar{r}) \gamma_j^r \cdot e^{ir\psi}$$

$$(2) \quad \Delta P(\bar{r}, \psi) = \sum_{m=-\infty}^{+\infty} \sum_{n=|m|+1, |m|+3, \dots}^{+\infty} \bar{P}_n^m(\nu) \bar{\tau}_n^m \cdot e^{im\psi}$$

where ν is an ellipsoidal coordinate and has relationship to non-dimensional radius \bar{r} as

$$(3) \quad \nu = \sqrt{1 - \bar{r}^2}$$

The total number of states from the rectangular method is $(2*M+1)*N$ where M is the maximum harmonic used and N is the number of polynomial used in the expansion.

The relationship between inflow and pressure states can be found in Ref. [4]. This relationship can be written in a complex form as below.

$$(4) \quad \{\gamma_n^m\} = (1/2V) \cdot [\bar{L}^e] \{\bar{\tau}_n^m\}$$

Induced Power Formulation

Induced power can be computed by multiplying inflow and pressure distribution across the rotor disk area.

$$(5) \quad C_P = \frac{1}{\pi} \int_0^{2\pi} \int_{r_{co}}^1 w \Delta P \cdot \bar{r} \cdot d\bar{r} d\psi$$

Substituting Eqs. (1) and (2) into Eq. (5) and solving for double integral yields the compact induced power equation below.

$$(6) \quad C_P = 2 \sum_m \sum_n \{\bar{\tau}_n^{-m}\}^T \{\gamma_n^m\}$$

Substituting Eq. (4) to (6) yields:

$$(7) \quad C_P = (1/V) \sum_m \sum_n \{\bar{\tau}_n^{-m}\}^T [\bar{L}^e] \{\bar{\tau}_n^m\} \\ = (1/V) \{\bar{\tau}\}^T [U] [\bar{L}^e] \{\bar{\tau}\}$$

Where $[U]$ is used to flip the order of $\{\bar{\tau}_n^{-m}\}$ so that $\{\bar{\tau}_n^{-m}\}^T = \{\bar{\tau}_n^m\}^T [U]$. Note that this complex form of the equations differs from Ref. [2] by a factor of 2.

Mass flow, V , is approximately equal to advance ratio, μ , in a high speed forward flight with skew angle close to 90°. $[\bar{L}^e]$ depends only on the skew angle. Therefore, Eq. (7) shows that the pressure states, $\{\bar{\tau}\}$, are the only required information to calculate the induced power.

Rotor Loads in Terms of Pressure States

Common loads in a helicopter are rotor thrust, roll moment, and pitch moment. (loads mean the six integrated rotor aero forces and moments) These loads can be represented with the pressure states, $\{\bar{\tau}\}$, as below

$$(8) \quad C_T = 1/\pi \int_0^{2\pi} \int_0^1 \Delta P \cdot \bar{r} \cdot d\bar{r} \cdot d\psi \\ C_L = -1/\pi \int_0^{2\pi} \int_0^1 \Delta P \cdot (\bar{r} \cdot \sin(\psi)) \cdot \bar{r} \cdot d\bar{r} \cdot d\psi \\ C_M = -1/\pi \int_0^{2\pi} \int_0^1 \Delta P \cdot (\bar{r} \cdot \cos(\psi)) \cdot \bar{r} \cdot d\bar{r} \cdot d\psi$$

Substituting pressure difference in Eq. (2) into (8) and solving for double integral yields:

$$(9) \quad \{C\} = [D] \{\bar{\tau}\}$$

where

$$(10) \quad [\bar{D}] = \begin{bmatrix} 0 & 2/\sqrt{3} & 0 \\ i\sqrt{2/15} & 0 & -i\sqrt{2/15} \\ -\sqrt{2/15} & 0 & -\sqrt{2/15} \end{bmatrix}$$

The analysis above assumes that the lift vector is perpendicular to the rotor disk plane rather than to the local air velocity vector. This is a reasonable assumption because a skew angle close to 90° makes the effect of the lift vector tilt negligible.

Blade Pitch Angle in Terms of Rotor-Control

Either higher-harmonic or radial rotor control causes the lift distribution along the blade to be altered as a function of azimuth. More control means having more ability to tailor the lift distribution into the ideal shape. Theoretically, having an infinite amount of control can reduce the induced power to Glauert's ideal power. Hall and Hall used infinite control (a rubber blade) in Ref. [9] and showed that the computed induced power approached the Glauert's ideal power as the number of blades was increases.

Typical examples of rotor-control are collective and cyclic pitch, higher harmonic control, blade twist, variable airfoil geometry and even circulation control through local blowing.

For this paper, we limit the rotor control vector $\{\bar{\theta}\}$ to be of the following form.

$$(11) \quad \theta(\bar{r}, \psi) = \sum_{h=-H}^{+H} \sum_{d=0}^D \bar{r}^d \bar{\theta}_d^h e^{ih\psi}$$

In addition, we include rotor shaft angle, α_s , as a control in the theory. Many rotor controls are possible with this form. Conventional collective and cyclic pitch control ($H = 1, D = 0$) is used as minimum control input in this present paper. Higher harmonic control results ($H > 1, D > 0$) will also be discussed in the result section.

Blade Element Lift in Terms of Rotor Pitch and Inflow

The rotor blade airfoil section airload, or lift per unit length, may be expressed in terms of the section velocity components U_P and U_T according to conventional blade-element theory.

$$(12) \quad L_q = (1/2)\rho ac[U_T^2 \cdot \theta - U_P \cdot U_T]$$

where U_T and U_P are

$$(13) \quad \begin{aligned} U_T &= \Omega R(\bar{r} + \mu \cdot \sin(\psi)) \\ U_P &= \Omega R(\lambda + w(\bar{r}, \psi)) \end{aligned}$$

Note that for present purposes of rotor performance analysis, rotor blade flapping motion is not included. In this present paper the lift curve slope, a , has a constant value, 6.0, with the assumption that the blade does not stall. Equations (12) - (13) show that induced inflow, $w(\bar{r}, \psi)$, changes the lift distribution, which consequently changes the induced power. Previous studies by File neglected the effect of inflow feedback in Refs. [2], [3]. This present paper shows that inflow feedback should not be neglected.

Pressure Loading in Terms of Rotor Controls

The relationship between pressure and blade sectional lift can be founded in Ref. [4]. Changing this relationship into a complex form yields:

$$(14) \quad \{\bar{\tau}\} = \frac{1}{2\pi} \int_0^1 L_q \phi_n^m(\bar{r}) \cdot d\bar{r} \cdot e^{-im\psi}$$

Substituting Eqs. (12) and (13) into Eq. (14) yields:

$$(15) \quad \{\bar{\tau}\} = \frac{\sigma a}{4} \cdot \left[\begin{aligned} &\int_{r_{co}}^1 (\bar{r} + \mu \sin(\psi))^2 [\theta(\bar{r}, \psi)] (\phi_n^m) d\bar{r} \\ &- \int_{r_{co}}^1 (\lambda + \mu \sin(\psi)) (\lambda + w(\bar{r}, \psi)) (\phi_n^m) d\bar{r} \end{aligned} \right] \cdot e^{-im\psi}$$

Changing sin and cos into their complex forms, substituting the pitch angle, induced inflow distribution (Eqs. (11) and (1)) into Eq. (15) yields:

$$(16) \quad \{\bar{\tau}\} = \frac{\sigma a}{4} \cdot \left[[\bar{A}]\{\bar{\theta}\} - [\bar{B}]\{\gamma\} \right]$$

Where

$$(17) \quad \{\bar{\theta}\} = \begin{Bmatrix} \vdots \\ \bar{\theta}_d^h \\ \vdots \\ \alpha_s \end{Bmatrix}$$

Where α_s is the nose up shaft angle and $\lambda = -\mu\alpha$.

Equation (16) involves pressure states, rotor control, and inflow states. Substituting inflow states, Eq. (4), into equation above simplify equation into pressure states in terms of rotor controls only.

$$(18) \quad \begin{aligned} \{\bar{\tau}\} &= \frac{\sigma a}{4} \cdot \left[[I] + \frac{\sigma a}{8V} [\bar{B}][\bar{L}^e] \right]^{-1} [\bar{A}]\{\bar{\theta}\} \\ &= [\bar{P}]\{\bar{\theta}\} \end{aligned}$$

where

$$(19) \quad [\bar{P}] = \frac{\sigma a}{4} \cdot \left[[I] + \frac{\sigma a}{8V} [\bar{B}][\bar{L}^e] \right]^{-1} [\bar{A}]$$

Note that the effect of induced inflow feedback, $[\bar{B}]$, is multiplied by the factor of $\frac{\sigma a}{8V}$. For a given values of lift curve slope, a , and mass flow V , solidity σ is the only parameter that determines the magnitude of the inflow feedback.

General Performance Problem – Rotor Power in Terms of Specified Controls

Equation (7) expresses power in terms of pressure states, $\bar{\tau}$. A few substitutions will yield the equation for rotor power in terms of rotor controls.

Substituting pressure states, $\bar{\tau}$, at Eq. (18) into Eq. (9) yields:

$$(20) \quad \{C\} = [\bar{D}][\bar{P}]\{\bar{\theta}\}$$

Where $\{C\}$ is comprised of rotor thrust and moments,

$$(21) \quad \begin{Bmatrix} C_T \\ C_L \\ C_M \end{Bmatrix} = [\bar{D}][\bar{P}]\{\bar{\theta}\}$$

Similarly, substituting pressure states, $\bar{\tau}$, at Eq. (18) into Eq. (7) yields:

$$(22) \quad C_P = (1/V)\{\bar{\theta}\}^T [\bar{P}]^T \{\bar{\theta}\}^T [U][\bar{L}^e][\bar{P}]\{\bar{\theta}\}$$

The expressions for C_T , C_L , C_M , and C_P provide rotor induced power for any specified rotor control inputs. This is a completely general analytical performance theory for all six rotor force and moment components, i.e., thrust, H-force, side force, roll and pitch moments, and shaft torque. Although Eq. (21) includes only three components; the development is easily extended to include the other three.

This result is notable in that it properly incorporates the complex non-uniform induced velocity distribution of the lifting rotor into a general analytical formulation for rotor induced power based on first-principles.

The induced power expressed analytically in Eq. (22) is analogous to Ormiston's quadratic power model of Refs. [8], [12], [13], however it is more direct, complete, and accurate than the numerical model based on computational results.

Induced Power Model

The quadratic power model of Refs. [8], [12], [13] expressed the induced power in terms of the most common basic rotor control variables of collective pitch, rotor angle of attack, and rotor blade linear twist. Six coefficients of this power model were termed power constants. They were obtained via parameter identification based on a database of numerical rotor power computations for a range of advance ratio. Blade element theory, linear airfoil aerodynamics, and Dynamic Inflow were used in these computations. Zero pitch and roll moments rotor trim was achieved with appropriate cyclic pitch.

Such a quadratic power model provides a simple means to quickly calculate rotor induced power as a function of advance ratio for arbitrary rotor controls. The results produced by this model are much more accurate compared to those calculated from the classical Glauert momentum theory based on uniform inflow.

The present analytical model may also be used to provide the power constants for the quadratic power model without the inconvenience and numerical inaccuracies noted in Refs. [8], [12], [13]. The following development will illustrate this process and provide typical results.

Specific conditions are chosen to study the general performance problem. Conventional collective and cyclic pitch are chosen as the three control variables, and edgewise flow was chosen as the flight condition. Edgewise flow condition implies small nose up shaft angle, α_s . From these conditions six power constants can be extracted.

Equation (22) can be rewritten as

$$(23) \quad \frac{C_P}{(\sigma a)^2} = (1/V)\{\bar{\theta}\}^T [\bar{P}]^T \{\bar{\theta}\}^T [U][\bar{L}^e][\bar{P}]\{\bar{\theta}\}$$

Where

$$(24) \quad [\bar{P}] = \frac{1}{\sigma a} [\bar{P}]$$

Expanding Eq. (23) yields

$$(25) \quad \frac{C_P}{(\sigma a)^2} = (1/\mu) \cdot \left(K_{\theta_0^2} \cdot (\theta_0)^2 + K_{\theta_c^2} \cdot (\theta_c)^2 + K_{\theta_s^2} \cdot (\theta_s)^2 + K_{\theta_0\theta_c} \cdot (\theta_0)(\theta_c) + K_{\theta_c\theta_s} \cdot (\theta_c)(\theta_s) + K_{\theta_0\theta_s} \cdot (\theta_0)(\theta_s) \right)$$

$K_{\theta_0^2}$, $K_{\theta_c^2}$, $K_{\theta_s^2}$, $K_{\theta_0\theta_c}$, $K_{\theta_c\theta_s}$, and $K_{\theta_0\theta_s}$ are the six power constants, and they are plotted versus advance ratio, μ , in Figs. 1 through 6. No root cut-out is used. The maximum harmonic number, $M=3$, and the number of polynomials, $N=100$, were used for a total of 700 states. The magnitude of inflow feedback is controlled by changes in the solidity value.

Note that these results cannot be compared directly with results in Refs. [8], [12], and [13] since they are for different conditions. In the present paper, the constants are partial derivatives with respect to the control variables: θ_0 , θ_s and θ_c . In Ref. [8], they are total derivatives with respect to collective pitch, shaft angle of attack, and blade twist under the constraint of a trimmed condition. For example, a variation in θ_0 in Ref. [8] implies corresponding variations in cyclic pitch to achieve the trim condition.

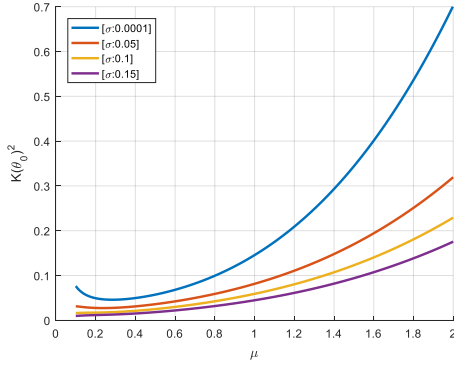


Figure 1. $K_{\theta_0^2}$, $M=3$, $N=100$

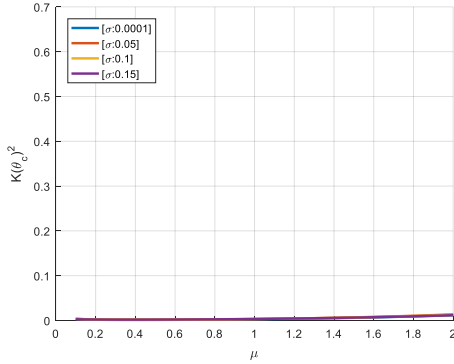


Figure 2. $K_{\theta_c^2}$, $M=3$, $N=100$.

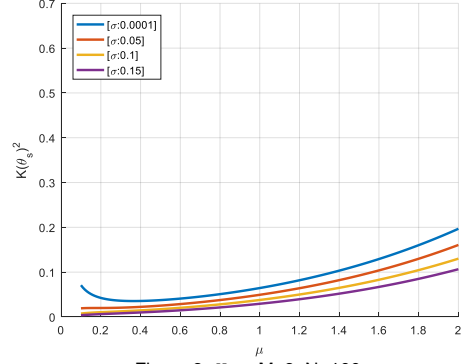


Figure 3. $K_{\theta_s^2}$, $M=3$, $N=100$.

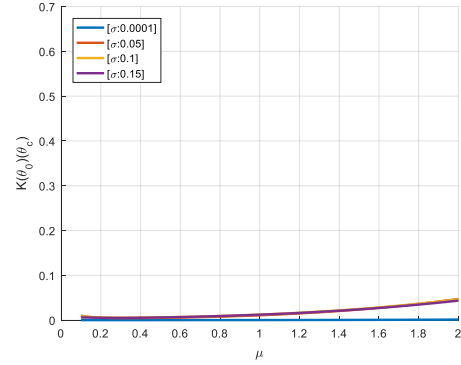


Figure 4. $K_{\theta_0\theta_c}$, $M=3$, $N=100$.

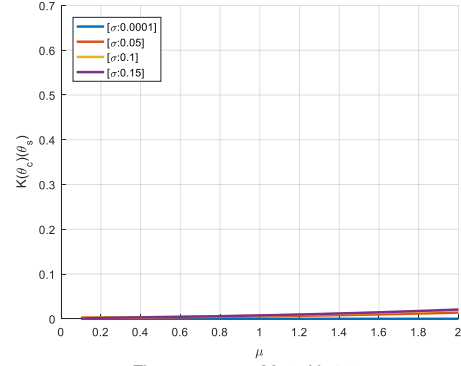


Figure 5. $K_{\theta_c\theta_s}$, $M=3$, $N=100$.

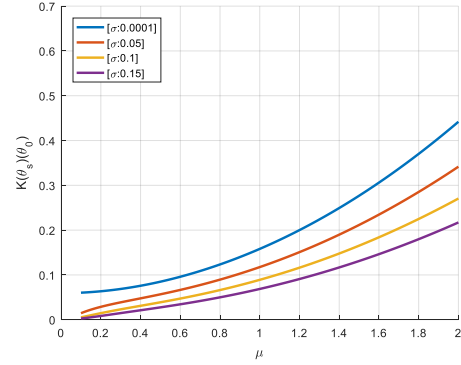


Figure 6. $K_{\theta_0\theta_s}$, $M=3$, $N=100$.

Optimum Performance Problem

Having presented the theory for the general performance problem, it is of interest to address the second problem discussed in the introduction — the inverse problem of determining the optimum control variables for minimum power.

Optimum performance for a helicopter rotor is typically defined for a specified trim condition; in the present work this generally means a given thrust with zero pitching and rolling moment values. These conditions are used as constraints for the induced power optimization.

The optimization procedure starts with definition of a functional $F(\bar{\tau})$, in terms of the induced power coefficient, C_P , with the dot product of the loading constraints, $\{C\}$, with Lagrange multipliers, $\{\bar{\Lambda}\}$.

$$(26) \quad F(\bar{\tau}) = C_P - \{C\}^T \{\bar{\Lambda}\}$$

Substituting Eqs. (7) and (9) into Eq. (19) yields:

$$(27) \quad F(\bar{\tau}) = \frac{1}{V} \{\bar{\tau}\}^T [U][\bar{L}^e] \{\bar{\tau}\} - \{\bar{\tau}\}^T \{\bar{D}\}^T \{\bar{\Lambda}\}$$

Substituting Eq. (19) into (27) yields:

$$(28) \quad F(\bar{\theta}) = \frac{1}{V} \{\bar{\theta}\}^T [\bar{P}]^T [U][\bar{L}^e][\bar{P}]\{\bar{\theta}\} - \{\bar{\theta}\}^T [\bar{P}]^T \{\bar{D}\}^T \{\bar{\Lambda}\}$$

Taking the variation of $F(\bar{\theta})$ and setting it equal to zero will give the optimality condition for C_P .

$$(29) \quad \delta F(\bar{\theta}) = \frac{1}{V} \{\delta\bar{\theta}\}^T [\bar{P}]^T [U][\bar{L}^e]_{sym} [\bar{P}]\{\bar{\theta}\} - \{\delta\bar{\theta}\}^T [\bar{P}]^T \{\bar{D}\}^T \{\bar{\Lambda}\}$$

where $[\bar{L}^e]_{sym}$ is the symmetric part of $[\bar{L}^e]$.

Optimum controls can be found from the above equation and they are:

$$(30) \quad \{\bar{\theta}\} = V([\bar{P}]^T [U][\bar{L}^e]_{sym} [\bar{P}])^{-1} [\bar{P}]^T \{\bar{D}\}^T \{\bar{\Lambda}\}$$

Solving for the Lagrange multipliers, $\{\bar{\Lambda}\}$, yields:

$$(31) \quad \{\bar{\Lambda}\} = \left(\frac{1}{V}\right) ([\bar{D}][\bar{P}]([\bar{P}]^T [U][\bar{L}^e]_{sym} [\bar{P}])^{-1} [\bar{P}]^T [\bar{D}]^T)^{-1} \{C\}$$

Equations (31), (30), (18), and (7) yield:

$$(32) \quad C_P = \left(\frac{1}{V}\right) \{C\}^T [\bar{Q}]^{-1} \{C\}$$

where

$$(33) \quad [\bar{Q}] = ([\bar{D}][\bar{P}]([\bar{P}]^T [U][\bar{L}^e]_{sym} [\bar{P}])^{-1} [\bar{P}]^T [\bar{D}]^T)$$

Normalization of the Power Equation

Since induced power is the power loss associated with the lift produced by the rotor, it is appropriate to normalize the induced power by the rotor thrust. This applies to the results for both the general rotor power problem, Eq. (22), as well as the optimum power problem, Eq. (32). For the optimum power problem, dividing both sides of Eq. (32) by C_T^2 yields:

$$(34) \quad \left(\frac{C_P}{C_T^2}\right) = \left(\frac{1}{V}\right) \left(\frac{\{C\}^T}{C_T}\right) [\bar{Q}]^{-1} \left(\frac{\{C\}}{C_T}\right)$$

$$\left(\frac{C_P}{C_T^2}\right) = \left(\frac{1}{V}\right) \{\bar{C}\}^T [\bar{Q}]^{-1} \{\bar{C}\}$$

Eq. (34) can be compared to the Glauert ideal induced power which is given by

$$(35) \quad \left(\frac{C_P}{C_T^2}\right)_{ideal} = \frac{1}{2\mu}$$

Equation (35) is the lowest possible induced power for high-speed forward flight of the lifting rotor. Therefore, calculated induced power should never be lower than the value of Eq. (35).

RESULTS WITH CLASSICAL CONVENTIONAL CONTROL

All of the results presented in this section use the following rotor blade configuration and flight conditions: infinite number of rectangular, untwisted blades, with conventional collective and cyclic pitch control and linear airfoil section lift-curve slope. The rotor blades are considered to be rigid without flapping hinges so that blade flapping motion is not included. Rotor angle of attack is zero and the lift is produced by collective pitch. The cyclic pitch is used to trim the rotor to zero resultant pitch and roll moment. A propulsive force trim constraint is not applied.

All plot titles include capital letters M, N, H, and D. M is maximum harmonic number and N is number of polynomials used. Both M and N are related to the convergence of the solution. Higher combinations of M and N produce more converged

solution. Solutions with $M=3$ and $N=100$ (700 states) can be considered as “fully converged.”

H is the maximum harmonic of blade pitch control and D is the maximum order of blade radial twist. In this section $H=1$ and $D=0$ are used. $D=0$ implies that the blade is untwisted.

Without Reverse Flow

To begin the analysis, we repeat the results of Refs. [2], [3], (with no reverse flow) but with more harmonics in the dynamic wake model than were used by File. Due to computer limitations and the presence of ill-conditioned matrices, File was only able to use eight harmonics in his analysis. Here, by using more efficient algorithms and by introducing conditioning enhancement, we have been able to obtain a fully converged solution.

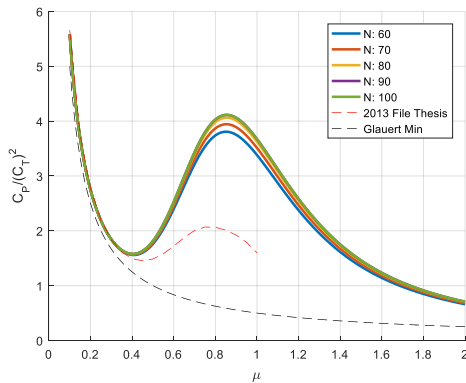


Figure 7. Fully converged induced power without reverse flow, $M=3$.

Figure 7 shows the comparison between the results of File and the present fully converged results. Even fully converged solutions do not show the singularity in power with no reverse flow. In other words, the power requirement does not go to infinity at the critical advance ratio.

Next, with no reverse flow, we compute induced power with different root cut-out (rco) values.

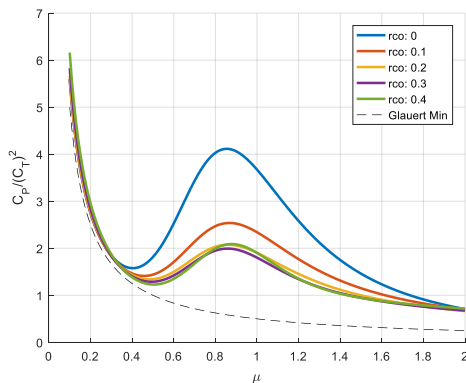


Figure 8. Effect of root cut-out without reverse flow, $M=3$, $N=100$.

Figure 8 shows that, as rco increases from zero to 0.3, the overall power consumption decreases. The reason behind this continuous reduction in power is related to how inflow and pressure are distributed throughout the rotor disk. For $rco \geq 0.4$ the power begins to increase.

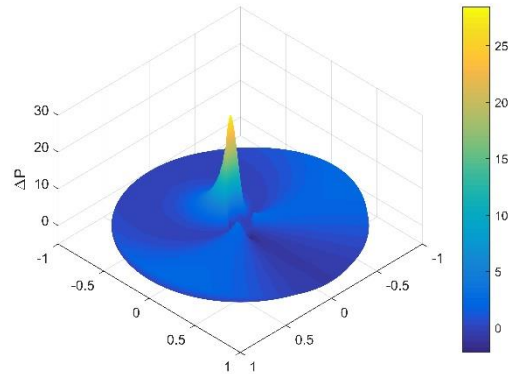


Figure 9. Pressure distribution across the disk with $rco=0.1$, advance ratio=0.9, $M=3$, $N=100$.

The pressure peak near the root region is shown in Fig. 9. The condition of small root cut-out and no reverse flow causes the pressure to be concentrated in a small region. High power consumption is caused by this small region because power is product of inflow and pressure distribution.

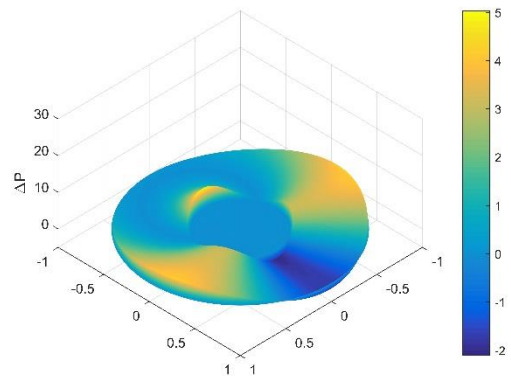


Figure 10. Pressure distribution across the disk with $rco=0.4$, advance ratio=0.9, $M=3$, $N=100$.

Applying moderate root cut-out removes this small region, causing the loads and inflow distribution to be spread out more evenly throughout the disk. Figure 10 shows how applying root cut-out value of 0.4 spreads out the pressure distribution compared to those in Fig. 9.

Effect of Reverse Flow

Figure 11 shows the induced power behavior when reverse flow is added to the model.

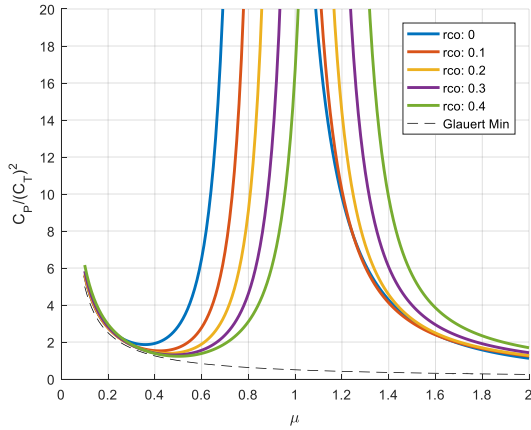


Figure 11. Effect of root-cutout with reverse flow, no inflow feedback, $M=3$, $N=100$.

The induced power becomes infinite near the critical advance ratio in the presence of reverse flow. This plot shows that direct analytical method can reproduce the singular behavior of the rotor power predicted by Ormiston and also confirmed by Hall and Giovanetti in Ref. [11]. Note that rotor angle of attack is zero and the rotor lift is produced by rotor collective pitch. Cyclic pitch is imposed to satisfy the zero hub moment trim condition. Advancing blade pitch decreases while retreating blade pitch increases.

As a result of this trim condition, inboard portion of the blade in the reverse flow region produces negative lift while the rest of the rotor produces positive lift. This highly non-uniform rotor lift distribution causes induced power to increase. In fact, at the critical advance ratio, the negative lift in the reverse flow region completely cancels the positive lift. The net lift response due to collective pitch control for trimmed hub moments is zero. In other words, at the critical advance ratio, the rotor is unable to trim to a nonzero rotor lift with collective pitch. However, the induced power remains positive and therefore the normalized induced power, $\frac{C_P}{C_T^2}$, becomes infinite.

Figure 11 also shows that changing the root cut-out shifts the critical advance ratio and the point of singularity. This makes physical sense in that, as root cut-out is increased, the region of reverse flow is diminished; and thus the critical advance ratio shifts to higher values with increasing root cut-out.

Effect of Inflow Feedback and Reverse Flow

The effect of inflow feedback is added to that of reverse flow in Fig. 12. The magnitude of inflow feedback is controlled by changes in the solidity.

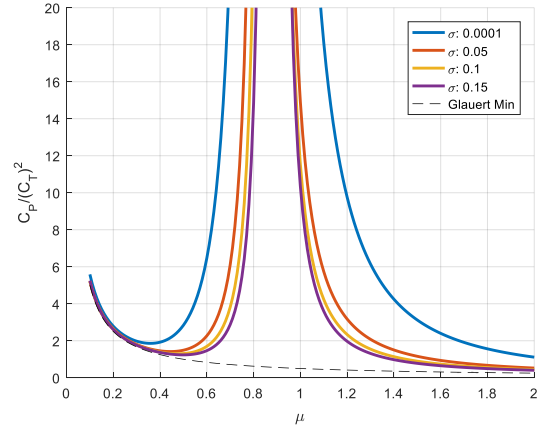


Figure 12. Effect of inflow feedback with reverse flow, no root cutout, $M=3$, $N=100$.

The overall induced power decreases with increased effect of inflow feedback (i.e., with increased solidity). The region of infinite power narrows when the solidity is increased. Inflow feedback forces the lift distribution into more ideal shape so that the induced power decreases.

RESULTS WITH HIGHER HARMONIC CONTROL

This section focuses on the effect of higher harmonic control. ($H \geq 1$ and $D \geq 0$) Other than that, analysis in this section uses same conditions as for the results for conventional control shown earlier.

Without Reverse Flow

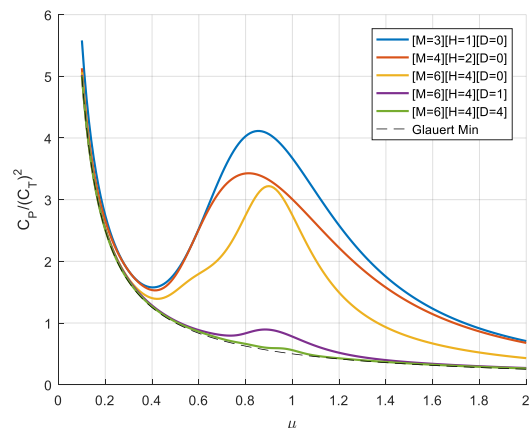


Figure 13. Effect of HHC control without reverse flow, no root cutout, $N=100$.

File showed that the power decreases with HHC control in Refs. [2], [3]. However, as seen from Fig. 7, his results were not fully converged. Fully converged HHC solutions are presented in Fig. 13. Application of more control degrees of freedom reduces the induced power, and it approaches the Glauert minimum.

Effect of Reverse Flow

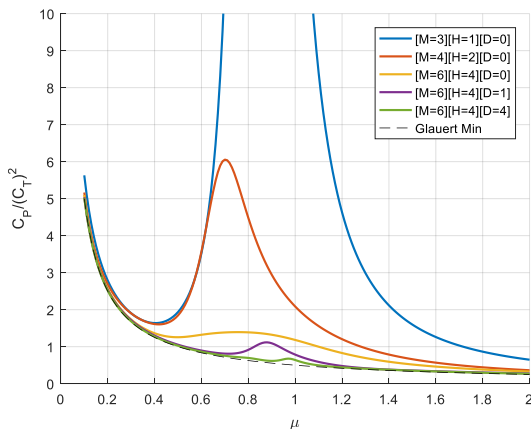


Figure 14. Effect of HHC control with reverse flow, no root cutout, $N=100$.

Figure 14 shows that HHC control removes the infinite power peak. Increasing H from 1 to 2 is enough to remove the singularity. Even with the presence of the reverse flow, using $H=4$ and $D=4$ brings the power curve down almost to the Glauert minimum.

Effect of Inflow Feedback and Reverse Flow

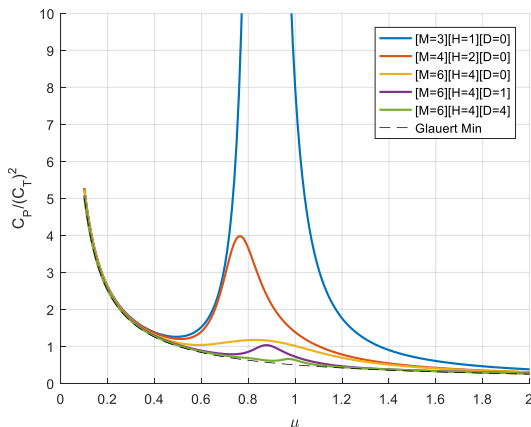


Figure 15. Effect of HHC control with reverse flow and inflow feedback, no root cutout, solidity=0.15, $N=10$.

Inflow feedback causes power peaks at Fig. 15 to be shorter and narrower compared to those at Fig. 14. Therefore, we can conclude that inflow feedback always reduces the induced power requirement. No

matter how many controls are used, inflow feedback will not increase the power consumption.

CONCLUSIONS

1. Finite state Dynamic Inflow provides a rigorous analytical model for lifting rotor performance in forward flight. The model is extended to include the effects of reverse flow and inflow feedback.

2. The model provides general performance characteristics for specified control variables as well as optimum performance subject to specified constraints.

3. The model also yields power constants for a quadratic power model that may be used to quickly calculate induced power as a function of advance ratio for specified rotor controls.

4. The present direct analytical method qualitatively reproduces the results found by Ormiston from numerical computation, including the singularity in normalized induced power.

5. Full solution convergence was achieved with more efficient algorithms and better conditioning enhancement than used by previous investigators.

6. With no reverse flow, moderate root cut-out reduces the induced power.

7. Reverse flow creates an infinite peak in normalized induced power due to the inability of a rotor at zero angle of attack to generate lift from collective pitch when trimmed to zero pitch and roll moments.

8. When the effect of reverse flow is added, root cut-out shifts the singularity to a higher μ .

9. The effect of inflow feedback reduces the induced power and narrows the region of infinite power.

10. Using higher harmonic controls decreases induced power in all three conditions: without reverse flow, with reverse flow, with inflow feedback and reverse flow. With a sufficient number of control degrees of freedom, the induced power approaches Glauert's minimum ideal power.

11. Higher harmonic control removes the infinite power peak caused by the reverse flow.

12. The reduction of induced power with inflow feedback is independent of the number of control used.

ACKNOWLEDGEMENTS

This work was sponsored by the GT/WU RCOE Program through an Army Contract, Dr. Mahendra Bhagwat Technical Monitor.

REFERENCES

1. Glauert, H., "A General Theory of the Autogyro," R&M No. 1111, Aeronautical Research Council of Great Britain, March 1927.

2. File, Chad, Peters, David A., and Ormiston, Robert A., "Optimum Rotor Performance with Realistic Constraints by Finite-State Induced Flow Methods," Proceedings of the 67th Annual National Forum of the American Helicopter Society, Virginia Beach, Virginia, May 3-5, 2011.

3. File, Chad L, *Optimization of Induced-Power from Dynamic Inflow Theory*, Ph.D. Dissertation, Washington University in St. Louis, May 2013.

4. He, Cheng Jian, *Development and Applications of a Generalized Dynamic Wake Theory for Lifting Rotors*, Ph.D. Dissertation, Georgia Institute of Technology, August 1989.

5. Harris, Franklin D., "Rotary Wing Aerodynamics Historical Perspectives and Important Issues," paper presented at the American Helicopter Society Southwest Region National Specialists' Meeting on Aerodynamics and Aeroacoustics, Arlington, TX, February 25-27, 1987.

6. Ormiston, Robert A., "Helicopter Rotor Induced Power," Proceedings of the AHS International 60th Annual Forum and Technology Display, Baltimore, MD, June 8-10, 2004.

7. Ormiston, Robert A., "Further Investigations of Helicopter Rotor Induced Power," Proceedings of the AHS International 61st Annual Forum and Technology Display, Grapevine, Texas, June 1-3, 2005.

8. Ormiston, Robert A., "A New Formulation for Lifting Rotor Performance Including Comparison

with Full-Scale Data," Proceedings of the AHS International 64th Annual Forum and Technology Display, Montreal, Quebec, Canada, April 29 - May 1, 2008.

9. Garcia-Duffy, Cristina, Peters, David A., and Ormiston, Robert A., "Optimum Rotor Performance in Skewed Flow Based on Actuator-Disk Theory," Proceedings of the 27th AIAA Applied Aerodynamics Conference, San Antonio, TX, June 22-25, 2009, AIAA- 2009-3517.

10. Hall, Kenneth C. and Hall, Steven R., "A Variational Method for Computing the Optimal Aerodynamic Performance of Conventional and Compound Helicopters," *Journal of the American Helicopter Society*, Vol. 55, No. 4, October, 2010, pp. 042006-1 through 042006-16.

11. Hall, Kenneth C. and Giovanetti, Eli B., "Minimum Power Requirements and Optimal Rotor Design for Conventional and Compound Helicopters Using Higher Harmonic Control," Proceedings of the 69th Annual National Forum of the American Helicopter Society, Phoenix, Arizona, May 21-23, 2013.

12. Ormiston, Robert A., "An Analytical Formulation for Lifting Rotor Induced Power, Proceedings of the AHS International 65th Annual Forum and Technology Display, Grapevine, TX, May 27-29, 2009.

13. Ormiston, Robert A., "Applications of the Induced Power Model and Performance of Conventional and Advanced Rotorcraft," Proceedings of the American Helicopter Society Aeromechanics Specialists' Conference, San Francisco, CA, January 20-22, 2010.